Two-dimensional phases of confined 5-cyano-biphenyl: Computer simulation study

Violetta Raczyńska, Krzysztof Górny ©, Przemysław Raczyński, and Zbigniew Dendzik ©[*]

Faculty of Science and Technology, University of Silesia in Katowice, ul. 75 Pułku Piechoty 1A, 41-500 Chorzów, Poland

Szymon Starzonek ©

Laboratory of Physics, Faculty of Electrical Engineering, University of Ljubljana, Tržaška 25, 1000 Ljubljana, Slovenia

The properties of composites of mesogens and two-dimensional (2D) materials are of great interest due to their practical applications in flexible displays, optoelectronics, microelectronics, and novel nanodevices. The properties of such composites are very complex and strongly depend on the interactions between the host material and the mesogen filling. We have performed molecular dynamics simulations for 4-cyano-4′-pentylbiphenyl embedded between graphene and hexagonal 2D boron nitride layers. The structural and dynamical properties of such systems were investigated in terms of the order parameters, density profiles, mean square displacement, and autocorrelation function of the single-molecule dipole moment. Our simulations have shown that the mesogenic molecules form highly stable ordered layered structures and that their dynamics are strongly related to the structural properties. We have investigated not only the effects of the polarization of the host material, but also the effects of the spatial repetition of such composites by using two models of mesogens embedded in 2D layers: the direct sheet and the structure formed by multiplying a single unit of the composite in the direction perpendicular to the substrate surface.

I. INTRODUCTION

The ambitious goal of physics is to model all observations in nature. This makes it possible to control or predict a phenomenon that can normally be verified experimentally. For the most part, physicists have focused primarily on equilibrium conditions and have not been able to deal with nonlinear phenomena. Unfortunately, virtually all behavior in nature is nonlinear and far from equilibrium. Therefore, physical predictions have been successful only in some cases of natural events. At present, physics is gradually penetrating into completely unconventional areas. It is noticeable that different phenomena are often connected by mathematical behavior; i.e., they are universal. Universalism, already postulated by Landau in the mid-20th century and by de Gennes in the 1980s, is a typical feature of complex systems (CS), which are in vogue in modern physics [1,2].

Computer simulations have been used to study the dipolar relaxation of polar molecules confined in a nanotube's inner cavity [3], properties of ultrathin layers of mesogens adsorbed at the nanotube surface [4], wetting of a crystalline substrate by nematic nanodroplets [5], and anchoring of mesogens on the surface of organic self-assembled monolayers [6]. It was shown that the quality of these self-assembled substrates significantly affects the arrangement of the mesogen layer and that the interface between the mesogen and the vacuum also significantly affects this ordering. Liquid crystals are sensitive to the processes that occur at interfaces.

There is research on liquid crystal systems doped with barium titanate nanoparticles ($BaTiO_3$) [7], silicon dioxide (SiO_2) [8], alumina oxide ($Al2O_3$) [9], carbon nanotubes (SWCNT) [10], and fullerene (C_{60}) [11], which is the starting point for this study. Thin mesogen films anchored on a variety of substrates have attracted considerable attention due to their extraordinary properties, which could find application in biochemical sensing devices [12] as well as optoelectronics [5,6]. Additionally, they have caused significant changes in the theoretical approach to the description of liquid crystals (LC). The optical properties of thin molecular layers (e.g., transparency) and the ability to switch easily and in a controlled manner between orientation configurations make them suitable materials for display devices and transistors. Significant development in the field of computer techniques, fostered by advances in accessible hardware, has enabled precise modeling of such systems [13,14].

The arrangement and alignment of liquid crystals determine the practicality of a mesogen-based device. Controlling the order of the system is one of the fundamental goals of liquid crystal research. Understanding the origin of such a mechanism at the molecular level is still insufficient. The orientation order and electrical and dielectric properties of liquid crystals can be strongly influenced by anchoring them on different substrates such as graphene [15] or carbon nanotubes [16]. The arrangement of 4-cyano-4′-pentylbiphenyl (5CB) mesogen films adsorbed on the surface of carbon nanotubes has been shown to exhibit odd-even effects, similar to the films adsorbed on the surface of silicon carbide nanotubes, while the latter system shows a more selective diffusion pattern [14].

In this work, we extend our previous studies on the effects of anchoring on the properties of ultrathin nCB films and the

---

[*]zbigniew.dendzik@us.edu.pl

effects of surface polarization of nanotubes by investigating the dynamics of 5CB phases embedded between nonpolar graphene and polar 2D boron nitride substrates. Undoubtedly, the presented results can be a good starting point for further consideration of the practical application of liquid crystal thin film systems. Previous research has shown the great potential of such systems for the design and construction of advanced antennas for telecommunications in 5G and 6G technology [17,18], thanks to the use of a nematic enclosed in micrometer cells of a polymer matrix. Furthermore, the use of thin LC films will be used in advanced optoelectronics as active lenses [19], as well as in electronics in the production of thermistors [20], *RC* filters [21], and supercapacitors [22]. The latter are of interest due to their potential application in modern devices for storing and converting energy [23,24]. Furthermore, the modeling of fluid film systems using LC can influence the development of fields such as molecular biology, medicine, and pharmacy, which focus on the study of the interaction of biological membranes with nanoparticles [25]. This field is currently being strongly developed by scientists from many disciplines. In view of this, extensive simulations of LC molecular dynamics in thin-film systems are justified.

II. SIMULATION DETAILS

We ran a series of molecular dynamics (MD) simulations using the NAMD 2.12 code [26]. Visualizations were performed using the VMD software [27]. Both the graphene sheet (GS) and the boron nitride sheet (BNS) were modeled as rigid bodies. The application of elastic models of the GS and BNS might lead to a slight decrease in the ordering of the mesogens near the substrate surface. Due to very similar unit cells of graphene and hexagonal boron nitride and very close atomic masses of the atoms (boron 10.81 amu, carbon 12.011 amu, nitrogen 14.0067 amu), the vibrations of both latices should be similar and affect the ordering to a very similar degree. Additionally, the reorientational dynamics of molecules, which should not be impacted by vibrations of the substrate, is dependent on the differences in timescales of the processes. The introduction of a rigid substrate allows direct comparison with our previous work, where we used rigid nanotube models [14,28], and other previously published results [5]. The interaction of BNS with the environment was modeled as described by Won and Aluru [29]. Polarization of the BNS surface was taken into account, and the partial charges were set at 0.4e for the B atoms and $-0.4e$ for the N atoms to reflect polarization of the BNS surface [29] The partial charges assigned to the BNS atoms were calculated for the polarization of BNS in water. 5CB mesogen molecules were described using a model developed by Tiberio *et al.* [13]. This is a united atom model that unifies CH, CH_2, and CH_3 groups into single interaction sited. The hexagonal boron nitride model has been used to study water transport in nanochannels [29], hexagonal boron nitride solvation in polar and nonpolar solvents [30], intercalation of boron nitride nanotubes (BNNTs) in phospholipid bilayers [31], and extraction of phospholipids from the bilayer [32]. The 5CB mesogen model, optimized for the correct prediction of the nematic isotropic phase transition in bulk samples, was used successfully to study the complex interaction between the

self-assembled monolayer and the 5CB film [6]. Nonbonded interactions were truncated at a distance of 15 Å. Long-range electrostatic interactions were modeled using the Ewald summation method with particle mesh [33]. Atomic motion equations were integrated using the Brunger-Brooks-Karplus algorithm [34]. In all investigated cases, the time step was set at 1 fs.

The initial configurations of the simulated system were obtained from NPT simulations (Langevin thermostat with dumping coefficient $\gamma = 1$ ps^{-1} and Nosé-Hoover Langevin barostat implemented in NAMD [26], $P = 1$ bar, $T = 350$ K, specific barostat oscillation time of 100 fs and Langevin piston decay of 50 fs) of GS or BNS in an isotropic 5CB reservoir. The mesogen reservoir was initially larger in the xy plane than the sheets by at least 15 Å in each direction. The excess 5CB molecules were removed from the simulation cell to obtain a uniform sample of mesogen molecules confined between the respective 2D substrates. We applied the geometrical criterion with respect to the center of mass of the 5CB molecule (molecules that lay outside the perpendicular box formed by GS or BNS were removed). After each exclusion of excess mesogen molecules, additional NVT simulations were performed to verify that the 5CBs formed a uniform sample. The systems were then used as initial configurations for the actual production NVT runs.

The confinements were modeled in two independent ways: double sheet-based gap (nonperiodic) and periodic boundary gap (periodic). The first model (nonperiodic) contained two substrate sheets in the simulation cell. In this case, the simulation cell was set at $9.1 \times 9.04 \times 15.0$ nm^3. The z dimension of the simulation box (15 nm) was chosen large enough to neglect interactions between the simulation cell and its images along the z axis. In the latter case (periodic model), a single sheet was used, and the gap was modeled by replicating the system along the z direction with periodic boundary conditions. This model corresponds to an infinite number of gaps arranged one on top of the other. The z dimension of the simulation box was adjusted to represent the thickness of the gap, while the other two dimensions were the same as for the nonperiodic model. The direct comparison of the nonperiodic and periodic models also allows us to check whether the periodicity of the gap (compositelike structure of several gaps) affects the order and dynamics of the molecules in the gap.

We considered gaps from 22 to 34 Å and simulated the systems at four temperatures: 290, 310, 330, and 350 K. Temperatures were selected to cover the bulk nematic state of 5CB and the nematic-isotropic liquid transition, which occurs around 327.1 K [35]. The number of 5CB molecules is constant for all samples with the same thickness, regardless of substrate type and model (393, 483, 553, and 643 for the slit thicknesses of 22, 26, 30, and 34 Å respectively). Before the production runs, each system was equilibrated for 10 ns. The 20 ns production runs were repeated five times, and the results were averaged over all trajectories obtained.

III. RESULTS AND DISCUSSION

The geometry of the system, i.e., the mesogenic phase confined between the sheets of 2D materials, affects the structure
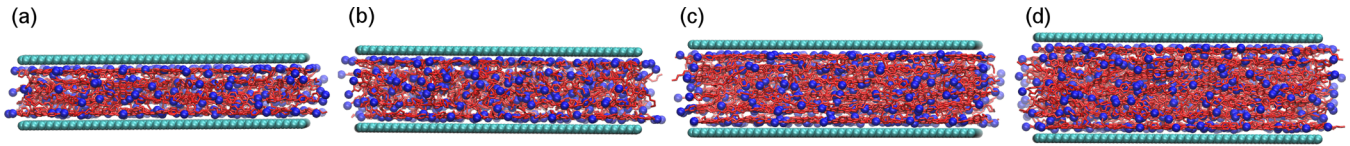
FIG. 1. Snapshots of final configurations of graphene single slit (nonperiodic model) at $T = 350$ K for (a) 22 Å, (b) 26 Å, (c) 30 Å, and (d) 36 Å width, filled with 5CB molecules; magenta (lighter) colored atoms correspond to the united atoms of the 5CB model, blue (darker) atoms are nitrogens.

and arrangement of the 5CB nematogens so that layers form parallel to the substrates. Layer formation is controlled by geometric constraints or available free volume, as well as by direct interactions between graphene or BNS sheets and 5CB molecules. Figures 1 and 2 show snapshots of graphene-based systems taken in the final stages of selected simulation runs for the nonperiodic and periodic models, respectively. In the case of the periodic system (see Fig. 2, top row), the images show the main simulation cell, while the bottom row shows two images of the simulation cell to visualize the formation of the gap due to the application of periodic boundary conditions. Additional orthogonal views of the large simulated graphene based slit are presented in Supplemental Material [36] Figs. S1 and S2 for nonperiodic and periodic slit models respectively. The 5CB layers adjacent to the 2D materials are clearly visible and denser than the layers formed in the nematic phase core. The number of 5CB layers formed depends on the thickness of the system (the distance between the graphene or BNS substrates that form the gap). We have chosen four gap thicknesses: about 22, 26, 30, and 34 Å, corresponding to 4, 5, 6, and 7 mesogenic layers, respectively.

In the course of the simulations, both 2D materials—graphene and BNS—induce ordered forms of the mesogens due to the substrate and geometric constraints. The number of layers was determined from the averaged surface density profiles shown in Fig. 3. The left panel shows the density profile in the case of the nonperiodic model, while the right panel shows the analogous profiles resulting from the periodic counterpart. In the latter case, the profiles have been shifted along the horizontal axis, and the data have been recalculated to make them comparable with the nonperiodic profiles. With

the exception of the central region, which is affected by the artifacts of this adjustment, the results of the periodic model agree well with those of the nonperiodic modeling. The peaks corresponding to the layers closest to the substrates are larger and better defined (in terms of half-widths) than in the case of the inner layers. In the latter case, the corresponding density profiles have lower magnitudes but are less defined, indicating that the inner layers are much thicker than the outer ones. This property is observed for 5CB molecules embedded in graphene or BNS gaps.

The orientation order of the ensemble can be characterized by the order parameter P_2, which describes the order of the liquid crystal molecules with respect to the director **n**. The values of P_2 and **n** can be calculated from the largest eigenvalue and the corresponding eigenvector of the order matrix **Q**, which is defined as follows [5]:

$$\mathbf{Q} = \left\langle \frac{\sum_{i=1}^{N}[3\hat{\mathbf{u}}_i(t) \otimes \hat{\mathbf{u}}_i(t) - \mathbf{I}]}{2N} \right\rangle, \tag{1}$$

where $\hat{\mathbf{u}}(t)$ is a unit vector along the selected molecular axis, **I** is the 3×3 identity matrix, **N** is the total number of mesogen molecules, and time averaging is performed over all available time steps of the trajectory. The principal axis of inertia was chosen for $\hat{\mathbf{u}}(t)$. The nematic order parameter P_2 of the mesogens as a function of the distance from the gap walls (the mesogen is divided into equal layers of thickness 4 Å and this spatial division does not correlate to the layers determined from the density profiles) for the case $d = 34$ Å is shown in Supplemental Material Fig. S1 [36]. The order of the nematic phases of 5CB near the graphene surface is slightly higher than in the case of BN surface: about 0.74. Although the
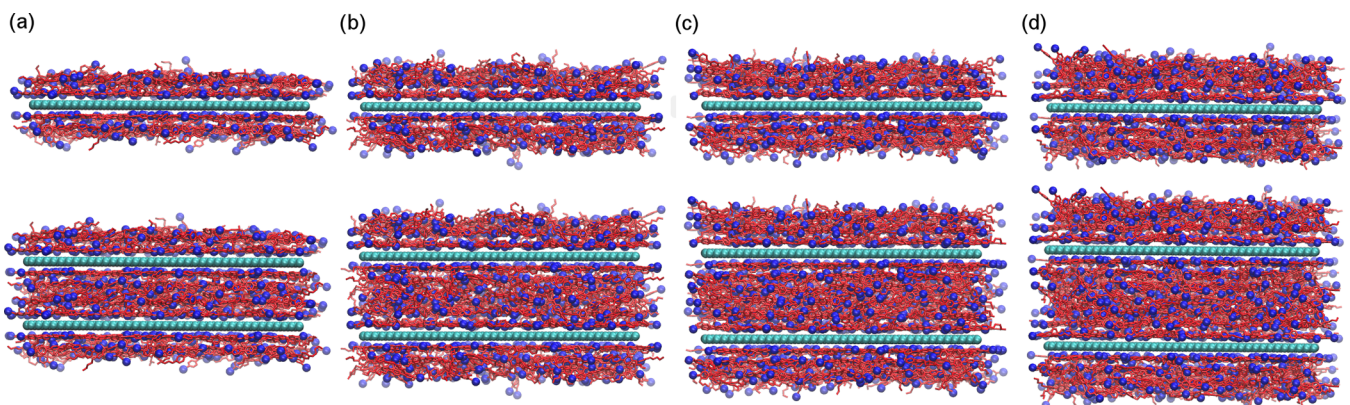

FIG. 2. Snapshots of final configurations of graphene slit (periodic model) at $T = 350$ K for (a) 22 Å, (b) 26 Å, (c) 30 Å, and (d) 36 Å width, filled with 5CB molecules; magenta (lighter) colored atoms correspond to the united atoms of 5CB model, blue (darker) atoms are nitrogens. Top view: single simulation cell; bottom view: fully formed slit obtained by repetition of the original cell in the z direction.
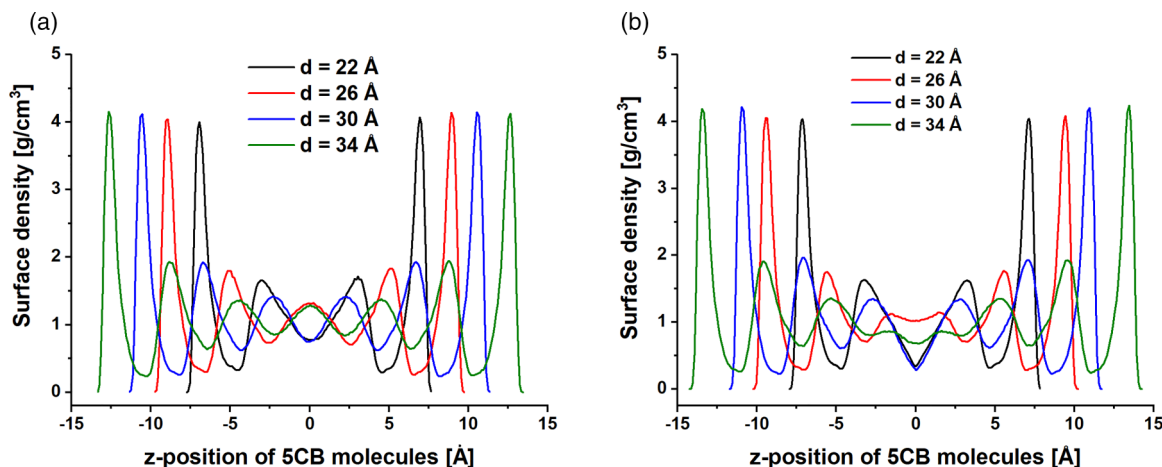
FIG. 3. Density profiles for graphene based phases at $T = 290$ K: left panel nonperiodic model, right panel periodic model, for different widths of the slit ranging from 22 (the narrowest profile) to 34 Å (the widest profile).

difference is rather small, it can be observed for both slit walls. This property also agrees well in the case of the non-periodic and periodic models. The nematic order decreases significantly in the middle of the slit. The order parameter for BN (ca. $P_2 = 0.48$) is lower than for its graphene counterpart (ca. $P_2 = 0.52$). Again, the difference applies both to the case where the gap is modeled directly and to the case where the gap is modeled with periodic boundary conditions.

The 5CB molecules within a single layer tend to arrange in parallel or antiparallel orientated groups, which are shown in Fig. 4. The molecules The left panel shows the layer closest to the substrate, while the right panel shows the snapshot of the instantaneous configuration of the mesogens in the central layer (furthest from the substrates). Both snapshots are for the graphene periodic 26 Å gap model. The inner layer is much thicker (lower panels) and more sparsely populated than the counterparts adjacent to the wall. This is related to the

conclusions on the density profiles: the inner layers are less pronounced and their half-widths are higher (Fig. 3).

Detailed representations of the order parameter P_2 in layers determined from density profiles (Fig. 3) are shown in Figs. 5 and 6 for the nonperiodic and periodic models, respectively. For each determined layer, the director was recalculated independently of the global director of the entire ensemble. The director was determined as the eigenvector corresponding to the highest eigenvalue of the order matrix 1. The P_2 parameter was then calculated only for the molecules forming the layer using the equation

$$P_2(\cos(\theta)) = \left\langle \tfrac{3}{2}\cos^2(\theta) - \tfrac{1}{2} \right\rangle, \qquad (2)$$

where θ is the angle between the director of the layer and the CN bond of the 5CB molecule. $\langle \rangle$ denotes the average of all molecules in the layer in all available time frames. The layers closest to the gap walls have a high degree of order. The ordering decreases with distance from the graphene surface. The parameter P_2 is generally higher in both models in the graphene-built gaps. This can be attributed to the higher uniformity and smoothness of the graphene surface compared to the BNS planes. Although the volume of the two gaps studied is almost identical, the number of layers formed between the graphene and BNS planes is not. The difference is in the central layers of the two smallest gaps (22 and 26 Å), where for graphene a weakly defined broad layer occurs and for BNS planes this single central layer can be split into two separate layers. The difference occurs in both the non-periodic and periodic models and can be associated with higher values of nonbonded interaction energy between the 5CB molecules and the BNS walls compared to the graphene-based gap. Values of the Lennard-Jones parameters are provided in Supplemental Material Table S1 [36]. Stronger van der Waals interactions partially eliminate the frustration of the 5CB molecules located in the center of the gap. This higher value of the nonbonded interaction is responsible for the 5CB layers being slightly closer to the plane surface in the case of BNS gaps, splitting the central layer into two separate layers (26 Å gap) or allowing the formation of an additional layer, as in the case of the narrowest gap (22 Å). This property is confirmed in both nonperiodic and periodic modeling of the slit. Only in the
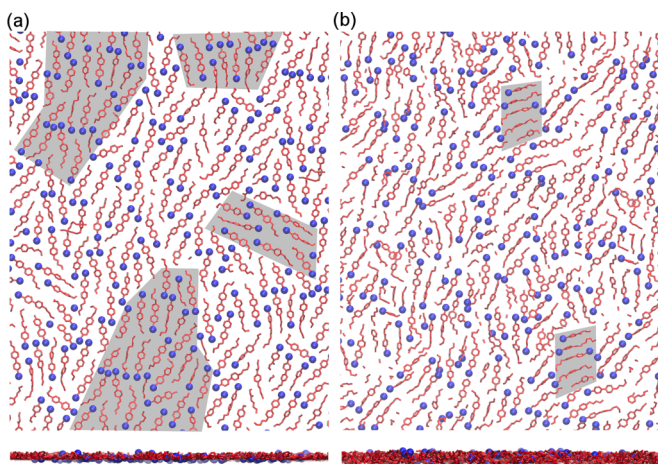

FIG. 4. Organization of 5CB molecules in one of the layers located between graphene layers at $T = 350$ K: (a) outermost layer (closest to graphene sheet), (b) innermost layer. Blue (darker) spheres represent nitrogen atoms from 5CB cyanide group. Exemplary domains of mesogens with similar orientation are highlighted in grey.
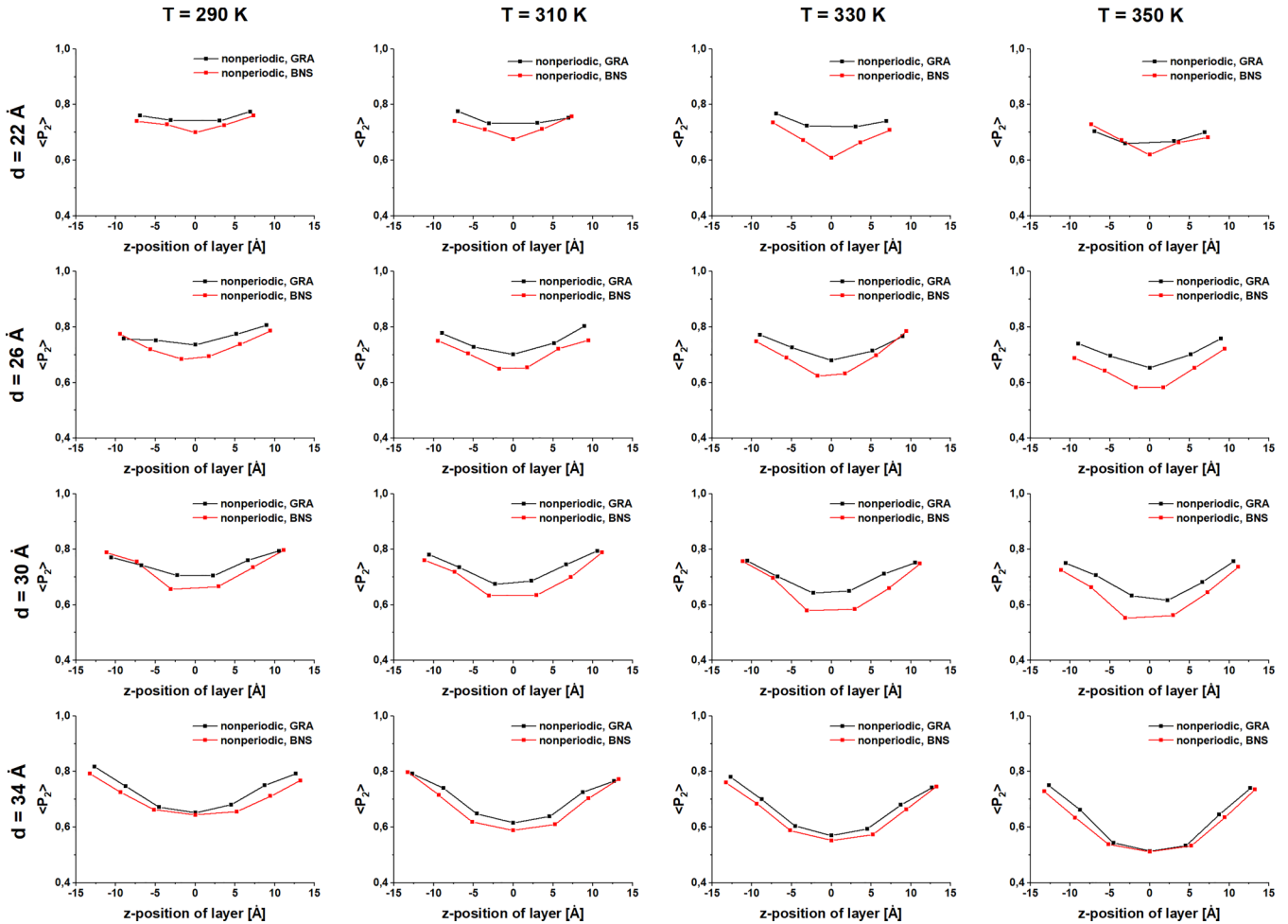
FIG. 5. Order parameters for distinct layers as a function of layer position for single slit model (nonperiodic).

case of the 26 Å gap, where the central layer is split into two layers in the case of the BNS gap, is a significant difference observed between the periodic and nonperiodic models. In the case of the nonperiodic model for graphene, the order of the central layer remains higher than in the case of 5CB layers located between BNS layers at similar positions. In the case of the periodic model, which is also continuous in the z direction, the order of the 5CB layers embedded between the graphene walls is lowered to the values observed for the BNS gap. In the case of the nonperiodic system, the partially polarized 5CB molecules tend to remain orientated in the plane, while, in the case of the periodic model, a more pronounced out-of-plane wobble of the director (in the z-axis direction) can be observed in the central layer, leading to overall lower values of the order parameter P_2. This could be related to the long-range electrical interactions of the system with its own copies, which try to minimize the overall dipole moment of the sample, leading to a broader distribution of molecular orientations.

The translational dynamics of 5CB molecules that form layers in the gap can be analyzed using diffusion coefficients D calculated from the mean square displacement (MSD) using the Einstein relation. The MSD was separated into two components: in plane (xy direction) and out of plane (z direction). The out-of-plane displacement is an order of magnitude smaller than the in-plane contribution. The upper panels of

Fig. 7 show the components in (left) and out (right) of the MSD in the plane for the 30 Å gap at $T = 310$ K. The out-of-plane translational dynamics reflects the differences between the nonperiodic and periodic models. In the case of the periodic model, the layers interact with their periodic boundary conditions (PBC) multiplied in the z direction, making the out-of-plane motion simpler and more pronounced. For both models, the out-of-plane displacement is smaller for gaps with graphene walls than for BNS-based gaps. The remaining panels show the geometric and temperature features of the MSD contribution in plane for the nonperiodic model. The mean displacement of 5CB molecules increases with temperature and gap size. Both models predict a similar shape of the MSD curves, so only the nonperiodic curves are presented. The translational dynamics of BNS-based slits are slightly more sensitive to system size and temperature, resulting in a larger scatter between the respective MSD curves.

The diffusion coefficients D obtained from the linear part of the MSD curves in the plane are given in the Table I (the part between 4 and 10 ns was fitted for all systems studied). The diffusion characteristic is almost insensitive to the type of substrate (graphene vs BN). The value of the diffusion coefficient increases with the size of the gap. In the case of the slit with $d = 26$ Å of the graphene-based slit, the inner-most layer has the lowest density and the highest available
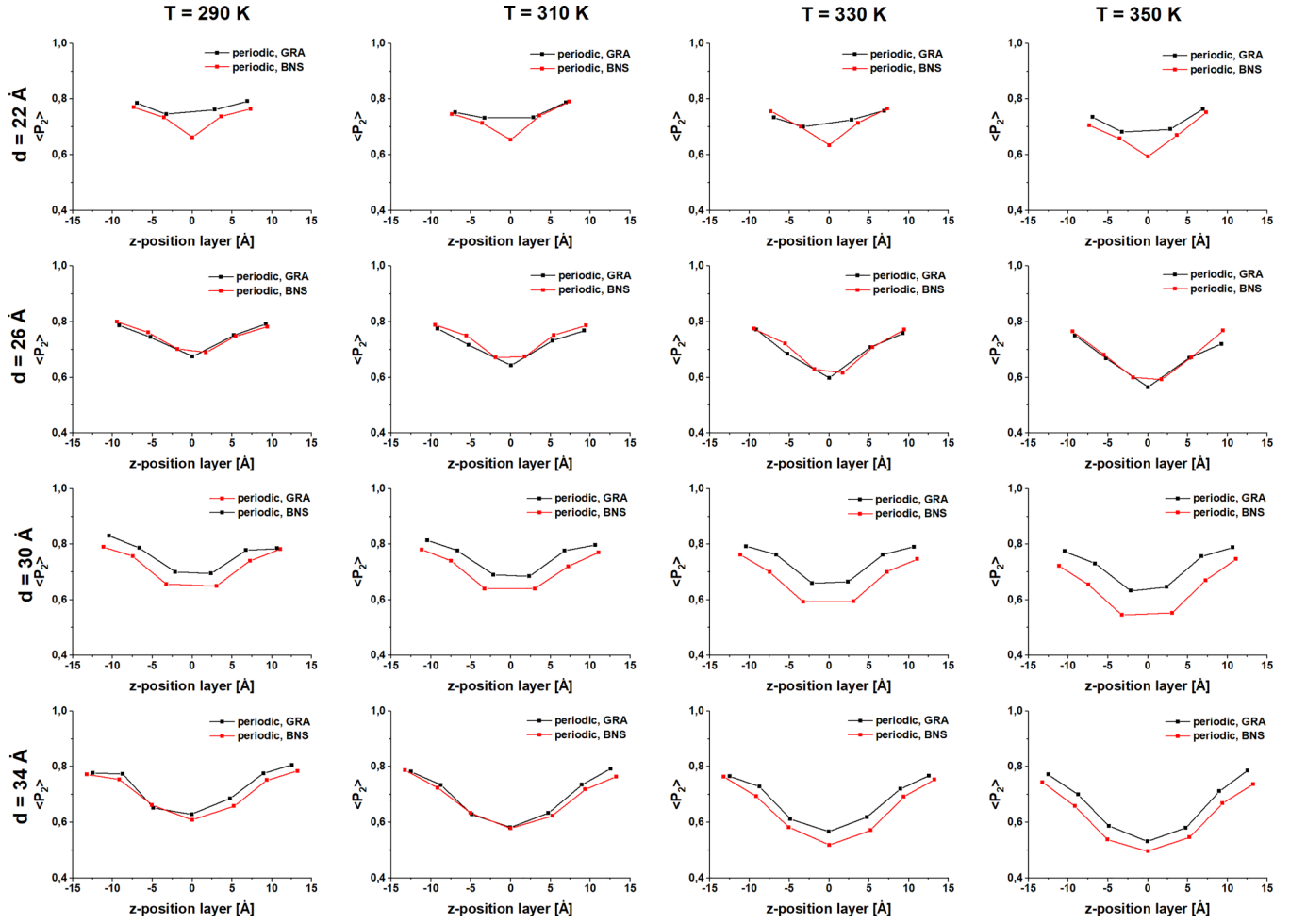
FIG. 6. Order parameters for distinct layers as a function of layer position for periodic slit model.

TABLE I. The values of diffusion coefficient D ($\text{Å}^2/\text{ps}$) (error smaller than 10% in all cases).

Size of the system	$T = 290$ K	$T = 310$ K	$T = 330$ K	$T = 350$ K
Nonperiodic model with graphene				
$d = 22$ Å	0.015	0.019	0.021	0.025
$d = 26$ Å	0.018	0.021	0.025	0.028
$d = 30$ Å	0.019	0.021	0.025	0.028
$d = 34$ Å	0.020	0.022	0.028	0.030
Nonperiodic model with BNS				
$d = 22$ Å	0.014	0.018	0.021	0.025
$d = 26$ Å	0.016	0.018	0.023	0.023
$d = 30$ Å	0.017	0.022	0.028	0.028
$d = 34$ Å	0.019	0.022	0.028	0.030
Periodic model with graphene				
$d = 22$ Å	0.016	0.019	0.021	0.022
$d = 26$ Å	0.020	0.025	0.028	0.030
$d = 30$ Å	0.018	0.020	0.025	0.030
$d = 34$ Å	0.021	0.025	0.028	0.030
Periodic model with BNS				
$d = 22$ Å	0.016	0.017	0.022	0.023
$d = 26$ Å	0.014	0.020	0.024	0.028
$d = 30$ Å	0.018	0.021	0.025	0.028
$d = 34$ Å	0.018	0.022	0.028	0.029

volume, leading to increased mobility of the molecules (see the Supplemental Material Figs. S4– S7 [36] for the effective density and boundaries of the 5CB layers). We checked the effective density of 5CB molecules to test whether the overall density of molecules in the 26 Å gap is perturbed and affects translational dynamics. We found no significant changes (see the Supplemental Material Table S2 [36]). The increased diffusion in the case of the 26 Å gap is the effect of the spontaneous organization of the 5CB molecules into layers, by their size and density. Obtained values of in-plane diffusion coefficients are in good agreement with values obtained for a bulk sample using a united atom model [37]. It should be noted that the values obtained using the united atom model are order of magnitude higher than values obtained experimentally using pulse-field-gradient spin-echo nuclear magnetic resonance (NMR) [38] or from all-atom simulations [37].

Reorientational dynamics of 5CB layers confined inside the graphene and BN gaps are analyzed in terms of the single molecular dipole moment autocorrelation function, defined as

$$\phi(t) = \frac{\langle \mu(t)\mu(0) \rangle}{\langle \mu(0)\mu(0) \rangle}, \qquad (3)$$

where μ denotes the dipole moment of the 5CB molecule and $\langle \, \rangle$ denotes the average over all available molecules and time
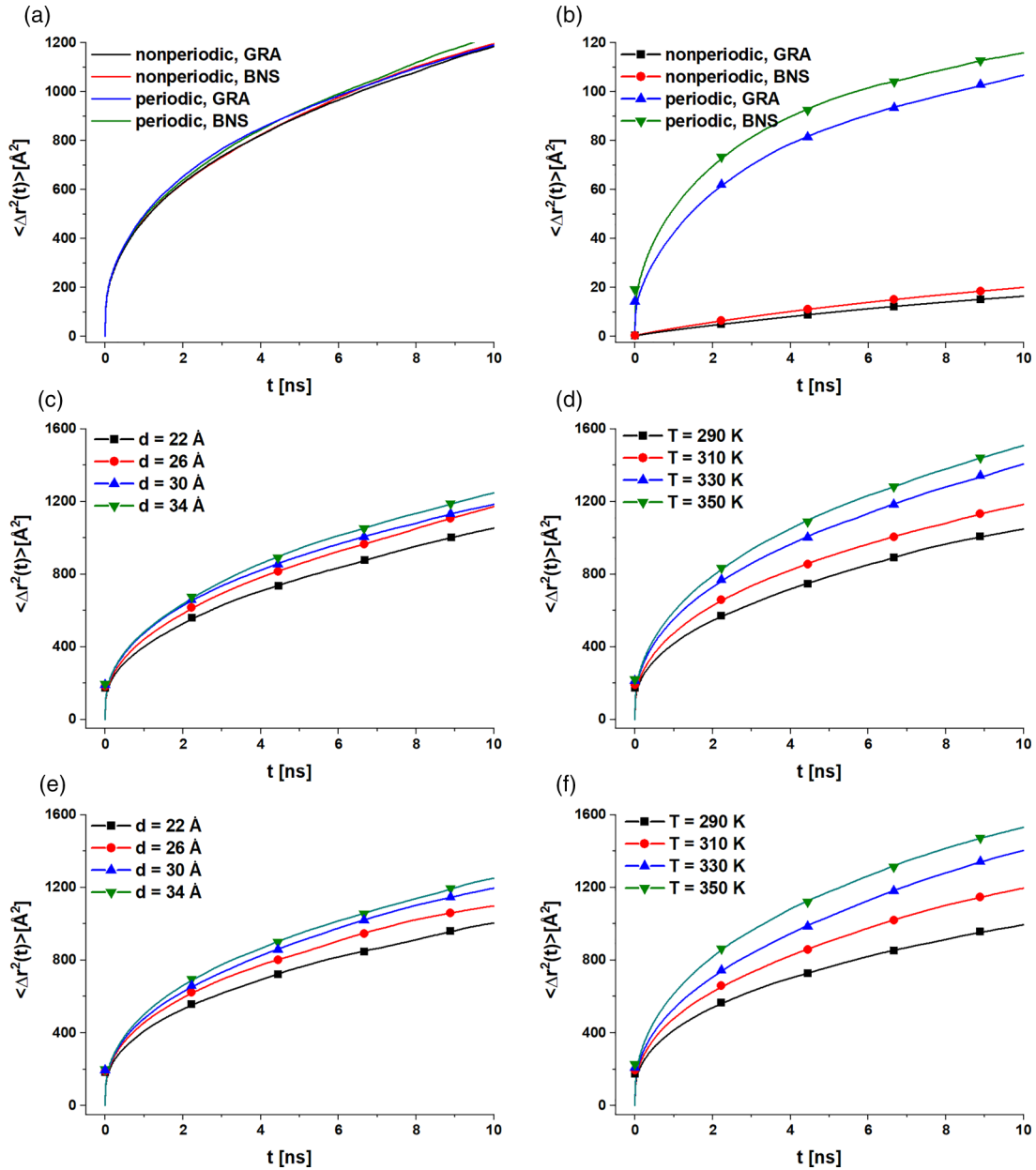
FIG. 7. MSD curves for 5CB molecules confined in slits: (a) in-plane (*xy*) component, (b) out-of-plane component, (c) size dependency of MSD for single graphene slit (nonperiodic model) at $T = 310$ K, (d) temperature dependency for nonperiodic system with width $d = 30$ Å, (e) size dependency of MSD for periodic graphene slit at $T = 310$ K, (f) temperature dependency for periodic system with width $d = 30$ Å.

origins. The layered structure prohibits the use of the total dipole moment correlation function, which could be successfully applied to single-molecule layers [14,28]. The layered structure and the fact that 5CB layers exchange molecules (MSD in the *z* direction reaches higher values than the largest distance between layers) leads to a complicated multiprocess relaxation of the total dipole moment. Furthermore, the dipole moments of the layers are not always aligned in the same direction and can relax independently, leading to the autocorrelation function of the total dipole moment varying between different simulation runs. In the case of single-molecule dipole moment relaxation, the process can be approximated by a single Kohlrausch-Williams-Watts (KWW) function defined

as follows:

$$\phi(t) = e^{-(t/\tau_{KWW})^{\beta}}, \qquad (4)$$

where τ_{KWW} is a measure of the characteristic relaxation time and $0 < \beta < 1$ is interpreted as a measure of the distribution of relaxation time or the cooperativity of the relaxation process. The mean relaxation time τ can be calculated using the following relation:

$$\tau = \int_0^{\infty} \phi(t)dt = \frac{\tau_{KWW}}{\beta}\Gamma\left(\frac{1}{\beta}\right), \qquad (5)$$

where Γ denotes the gamma Euler function. The parameters obtained from the KWW fits for all the cases studied are
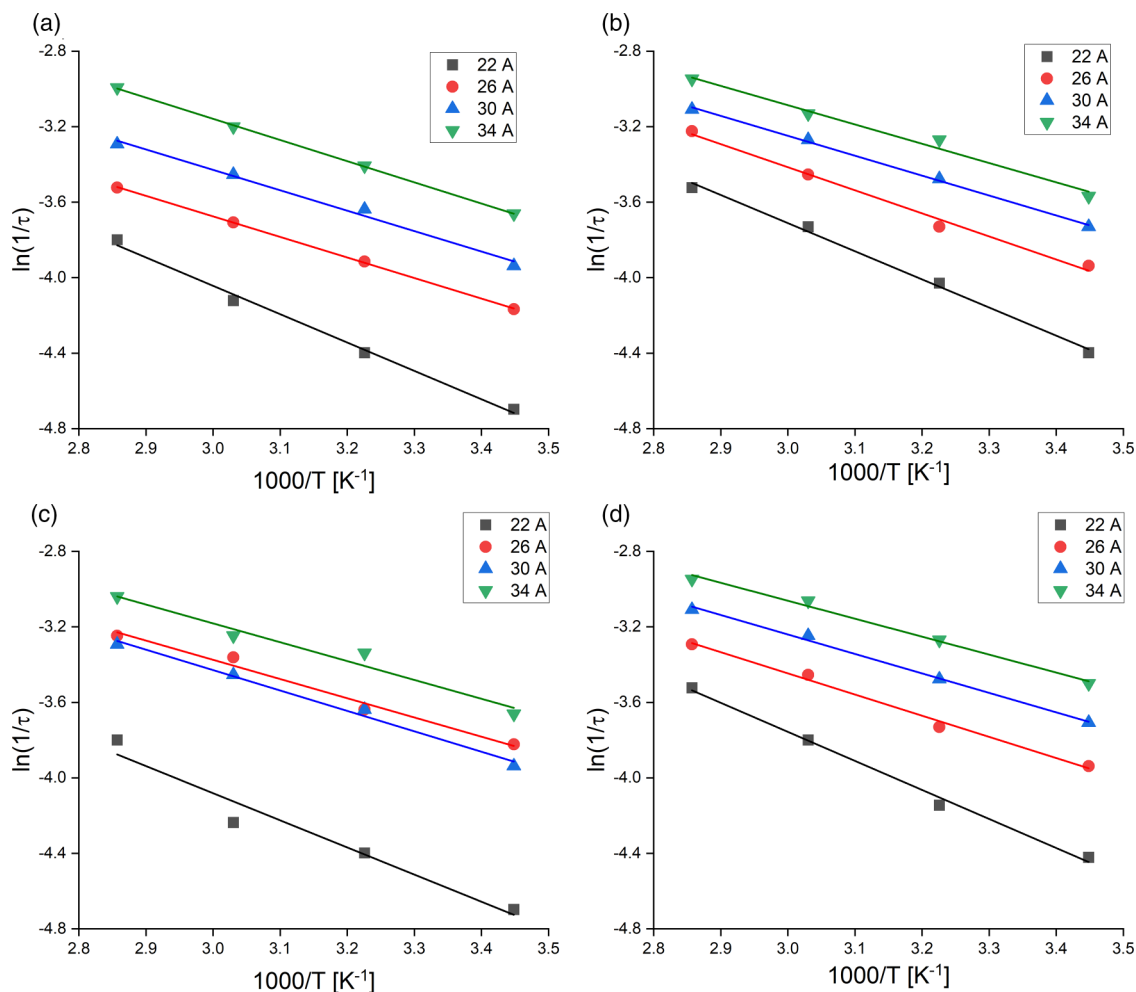
FIG. 8. Activation plots of single molecule dipole moment reorientational relaxation for single slit non-periodic model with a) graphene substrate, b) BNS substrate and periodic slit model with c) graphene substrate or d) BNS substrate. The scale on y axis is ps^{-1} as the relaxation time is measured in ps.

presented in the Supplemental Material [36] (Table S3). The relation between diffusion coefficient and relaxation time was established in a previous study [39]. It was shown that that $D \propto 1/\tau$. Therefore, the activation of diffusion shows a trend similar to that presented in Fig. 8.

Figure 8 shows the temperature dependence of the mean relaxation time (activation diagram) and the fitted KWW curves for the nonperiodic and periodic models. In the case of the narrowest 22 Å gap, the temperature characteristic differs significantly from that of wider gaps: the relaxation is significantly slower and the slope of the curve is different, indicating a stronger temperature dependence and a higher energy barrier for the rotational dynamics. The dynamics in systems with a graphene substrate is slower than in the case of BNS-based gaps. Both the nonperiodic and periodic models predict very similar reorientation dynamics of 5CB molecules embedded in gaps. The only outlier, as with the order parameter, is the 26 Å gap embedded on a graphene substrate. In the case of the periodic model, the relaxation times are shorter than in the nonperiodic case. The acceleration of the dynamics in this case is significant enough to exceed that observed in the case of the wider 30 Å gap. To further investigate the reorientation dynamics and structural relaxation of

the 5CB layers embedded in the gap, we decided to visualize the orientation of the director of the layers adjacent to the inner walls and the gap of 5CB molecules. The results for the narrowest and the widest gaps are shown in Figs. S8 and S9 of the Supplemental Material [36]. The results are shown for the lowest temperature studied and indicate that the director of the layers adjacent to the gap wall remains relatively stable during the simulation time and shows a concentration around selected points. The directors of the innermost layer(s) fluctuate more, and the features have a greater directional distribution. The director is able to leave the layer plane to a greater extent. The amplitude of the out-of-plane motions increases with the slit size and is almost independent of the substrate type and the slit model. The only significant difference occurs in the size of the periodic model gap of 26 Å size (Supplemental Material Fig. S10 [36]). The movement of the director of the inner layer(s) is more confined to the plane of the layer in the case of the periodic gap. This behavior is more pronounced in the case of the graphene-based periodic gap than in the case of the BNS gap, where the in-plane and out-of-plane motions are almost equal. In the case of the graphene-based gap, the precession of the director in the inner layer is practically confined to the plane of the layer. This finding suggests that, although the
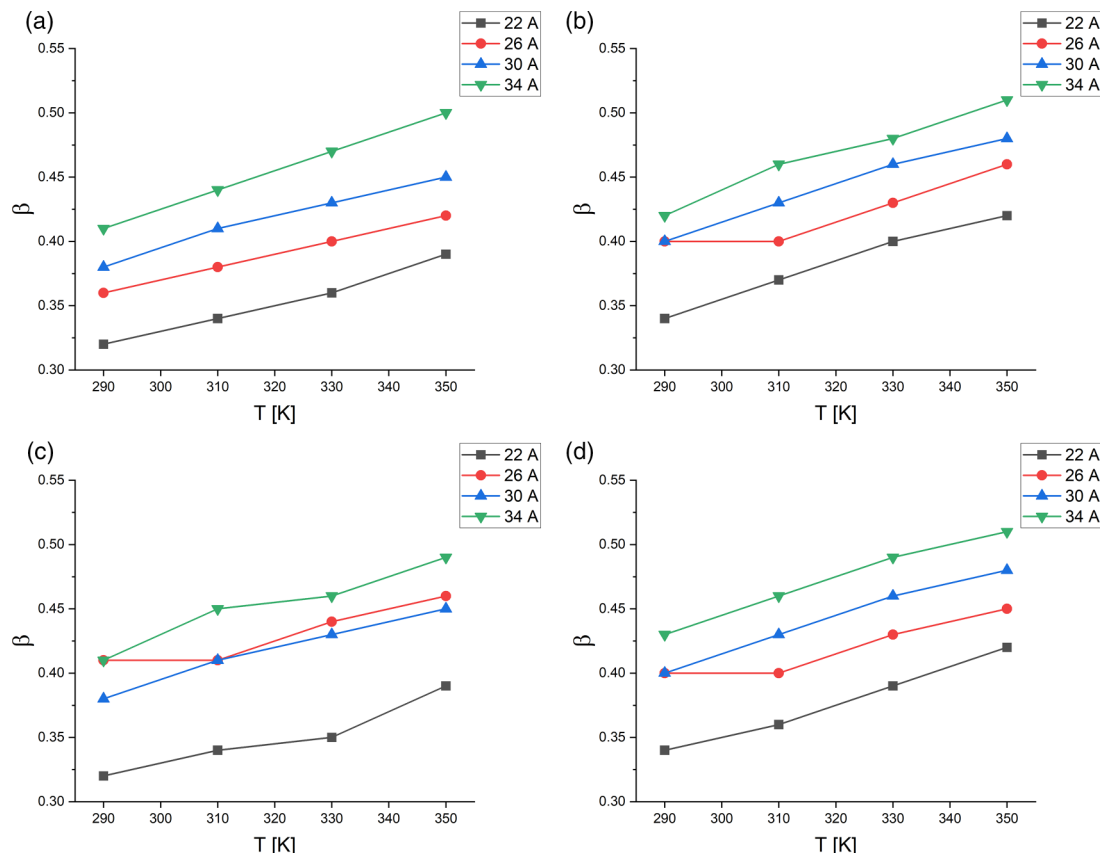
FIG. 9. Temperature dependency of β parameter describing distribution of relaxation times for single slit non-periodic model with a) graphene substrate, b) BNS substrate and periodic slit model with c) graphene substrate or d) BNS substrate.

density of the layers in the gap is not significantly different, the dynamics of the molecules is different for periodic model gaps of this size. The molecules in the inner layer reorient in the plane, leading to the accelerated dynamics observed for the periodic model of the 26 Å graphene slit.

The parameter β of the KWW fit, which represents the broadening of the distribution of relaxation times, fitted to the autocorrelation function of the dipole moment of a single molecule, is shown in Fig. 9. The value of β increases with temperature, indicating a transition from cooperative relaxation to a single-molecule process with a narrower distribution of relaxation times. β also increases with the width of the gap. The narrowest gaps have the slowest relaxation of reorientation with the lowest values of β. This can be explained by the predominant role of the 5CB molecules, which are directly adjacent to the gap walls, in the relaxation process. In the narrowest slit, the number of molecules in the densest layers represents a significant part of the population. Due to the high density of the layer and the high degree of order, molecules cannot reorient themselves independently, but only cooperative movements of groups of molecules are possible, which leads to an increase in the relaxation time τ and a decrease in the values of β. The reported values of β agree well with those determined in [28]. In contrast to the relaxation times discussed in the previous section, there is no significant difference between the graphene and BNS substrates.

Figure 10 presents the activation energies of single-molecule dipole relaxation (E_A) calculated for all sizes and types of cleavage substrates considered for both nonperiodic and periodic models. In the case of BNS-based gaps, the activation energy of the single-molecule relaxation decreases with the size of the gap. The graphene-based gap shows a more interesting property. The smallest gap, where the number of molecules physisorbed on the graphene surface represents a significant number of the total molecules, has the highest activation energy, while the activation energy seems to stabiliZe at a certain level as the gap size increases, and the increase in the gap size does not seem to affect the activation energy anymore. This behavior can be confirmed for both models considered. This fact suggests that the stabilisation of the activation energy of the single-molecule reorientation is mainly driven by the short-range van der Walls interactions between the layers, while the Coulombic interactions with the polariZed BNS substrate lead to a monotonic decrease of E_A. The layers physisorbed to graphene exhibit slower reorientation dynamics, and this fact is also reflected in the average values of the mean relaxation time of the single-molecule dipole autocorrelation function (see Table S3 in the Supplemental Material [36]). Except for the narrowest periodic model graphene gap, the activation energy values E_A are lower in the case of periodic slit than in the case of its nonperiodic counterpart, which can be attributed to electrostatic interactions with the self-images of PBC. In our previous studies [14,28], we estimate that the activation energy of dipolar relaxation of a single molecule thick layer of 5CB located on different nanotube surfaces is in the range of 50 to 65 kJ/mol. This value
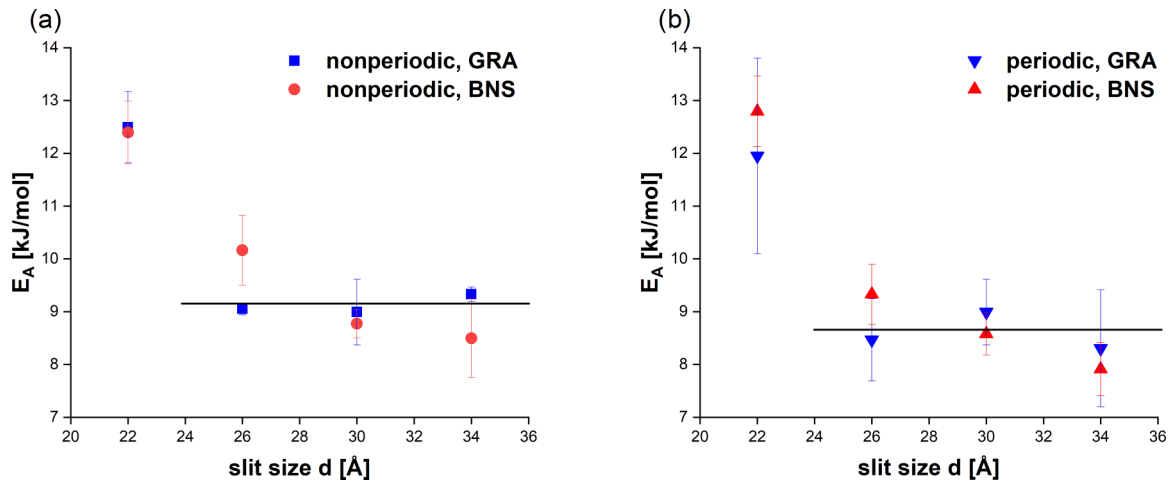
FIG. 10. Activation energy of single-molecular dipole moment relaxation for 5CB nematic phases between graphene and BNS surfaces. Lines are guides for eyes only.

is higher than the activation energy of the autocorrelation of the dipole moment of a single molecule reported here for the gaps. However, this can be understood in terms of comparing a cooperative, complex process involving several molecules with the reorientation dynamics of a single molecule.

IV. CONCLUSIONS

5CB molecules embedded in graphene and BNS gaps spontaneously form layered structures. The orientation of the molecules is always parallel to the gap walls for the investigated gap widths. The layers that form near the substrate have the highest density and are the most ordered. The order parameter for the layers decreases significantly with distance from the gap walls, although it should be noted that the values obtained of P_2 indicate that even the innermost layers maintain a nematic order and do not show a transition to the liquid phase even at temperatures of 350 K. The density of the layers also decreases with distance from the gap wall, and the innermost layers are not only more disordered but also thicker than their outermost counterparts. In the case of very thin gaps, the number of molecular layers can be influenced by the applied model of the slit. The presence of periodic images of the cleft could lead to the formation of additional layers of nematic molecules by splitting existing layers. It should also be noted that the application of a polar BNS gap substrate may lead to the formation of a higher number of layers compared to that of nonpolar graphene.

The translational motion of the molecules in the plane is very similar in all of the systems studied. However, there is a difference in the exchange of molecules between the nonperiodic and periodic models. In the case of the periodic system, the mean-square displacement of the molecules in the out-of-plane direction is almost an order of magnitude higher than in the case of the nonperiodic models. In contrast, the rotational dynamics is not affected as much by the gap model. Nonperiodic and periodic slit models predict a very similar characteristic of the relaxation times for the autocorrelation function of the single-molecule dipoles. On the other hand, the polarity of the cleavage substrate plays an important role. For polar BNS substrate gaps, the reorientation dynamics is faster and is less dependent on the gap size. The activation energy of relaxation of reorientation in the case of polar BNS gaps is much less influenced by the dynamics of the outermost layers and decreases with the size of the gap, while in the case of nonpolar graphene the 22 Å gap is dominated by the outermost layers and is much higher than other investigated gap widths, which maintain a stable activation energy regardless of the size of the gap.

[1] P. de Gennes and J. Prost, *The Physics of Liquid Crystals*, International Series of Monographs on Physics (Clarendon, Oxford, 1993)

[2] C. Zannoni, *Liquid Crystals and Their Computer Simulations* (Cambridge University Press, Cambridge, 2022)

[3] Z. Dendzik, K. Górny, and Z. Gburski, Cooperative dipolar relaxation of a glycerol molecular cluster in nanoscale confinement—a computer simulation study, J. Phys.: Condens. Matter **21**, 425101 (2009).

[4] A. Dawid and W. Gwizdała, Dynamical and structural properties of 4-cyano-4-n-pentylbiphenyl (5CB) molecules adsorbed on carbon nanotubes of different chiralities: Computer simulation, J. Non-Cryst. Solids **355**, 1302 (2009), special issue, Functional and Nanostructured Materials.

[5] O. M. Roscioni, L. Muccioli, R. G. Della Valle, A. Pizzirusso, M. Ricci, and C. Zannoni, Predicting the anchoring of liquid crystals at a solid surface: 5-cyanobiphenyl on cristobalite and glassy silica surfaces of increasing roughness, Langmuir **29**, 8950 (2013).

[6] O. M. Roscioni, L. Muccioli, and C. Zannoni, Predicting the conditions for homeotropic anchoring of liquid crystals at a soft surface. 4-n-pentyl-4'-cyanobiphenyl on alkylsilane self-assembled monolayers, ACS Appl. Mater. Interfaces **9**, 11993 (2017).

[7] J. Łoś, A. Drozd-Rzoska, S. J. Rzoska, S. Starzonek, and K. Czupryński, The fluctuation-driven dielectric properties of liquid crystalline 8OCB and its nanocolloids, Soft Matter **18**, 4502 (2022).

[8] D. Beroguiaa, F. Z. Abdoune, Z. H. Belaid, and L. Méchernène, Influence of SiO_2 nanoparticles on electro-optical and thermophysical properties of polyacrylate/liquid crystal composites, Liq. Cryst. **47**, 799 (2020).

[9] N. Yadav, R. Dabrowski, and R. Dhar, Effect of alumina nanoparticles on dielectric permittivity, electrical conductivity, director relaxation frequency, threshold and switching voltages of a nematic liquid crystalline material, Liq. Cryst. **41**, 1803 (2014).

[10] I. Dierking, G. Scalia, and P. Morales, Liquid crystal–carbon nanotube dispersions, J. Appl. Phys. **97**, 044309 (2005).

[11] S. J. Rzoska, S. Starzonek, J. Łoś, A. Drozd-Rzoska, and S. Kralj, Dynamics and pretransitional effects in C_{60} fullerene nanoparticles and liquid crystalline dodecyl-cyanobiphenyl (12CB) hybrid system, Nanomaterials **10**, 2343 (2020).

[12] J. A. Moreno-Razo, E. J. Sambriski, N. L. Abbott, J. P. Hernandez-Ortiz, and J. J. de Pablo, Liquid-crystal-mediated self-assembly at nanodroplet interfaces, Nature (London) **485**, 86 (2012).

[13] G. Tiberio, L. Muccioli, R. Berardi, and C. Zannoni, Towards *in silico* liquid crystals. realistic transition temperatures and physical properties for *n*-cyanobiphenyls via molecular dynamics simulations, ChemPhysChem **10**, 125 (2009).

[14] K. Gorny, P. Raczynski, Z. Dendzik, and Z. Gburski, Odd–even effects in the dynamics of liquid crystalline thin films on the surface of single walled carbon and silicon carbide nanotubes: Computer simulation study, J. Phys. Chem. C **119**, 19266 (2015).

[15] T. M. Alam and C. J. Pearce, Impact of graphene incorporation on the orientational order of graphene/liquid crystal composites, Chem. Phys. Lett. **592**, 7 (2014).

[16] V. Manjuladevi, R. K. Gupta, and S. Kumar, Effect of functionalized carbon nanotube on electro-optic and dielectric properties of a liquid crystal, J. Mol. Liq. **171**, 60 (2012).

[17] Z. Zhou, W. Li, J. Qian, W. Liu, Y. Wang, X. Zhang, Q. Guo, Y. Yashchyshyn, Q. Wang, Y. Shi, and Y. Zhang, Flexible liquid crystal polymer technologies from microwave to terahertz frequencies, Molecules **27**, 1336 (2022).

[18] G. Perez-Palomino, E. Carrasco, M. Caño-Garcia, R. Hervás, X. Quintana, and M. A. Geday, Design and evaluation of liquid crystal-based pixels for millimeter and sub-millimeter electrically addressable spatial wave modulators, in *2019 International Conference on Electromagnetics in Advanced Applications (ICEAA)* (IEEE, Piscataway, 2019), pp. 0787–0787.

[19] N. Bennis, T. Jankowski, O. Strzezysz, A. Pakuła, D. C. Zografopoulos, P. Perkowski, J. M. Sánchez-Pena, J. M. López-Higuera, and J. Algorri, A high birefringence liquid crystal for lenses with large aperture, Sci. Rep. **12**, 14603 (2022).

[20] M. M. Mohan, Dielectric relaxations in a liquid crystal along with thermistor application, The Eur. Phys. J. E **45**, 97 (2022).

[21] P. J. Perkowski, Low-pass RC filter modified by liquid crystal exhibiting one Debye relaxation: theoretical approach, Opto-Electron. Rev. **30**, e141949 (2022).

[22] R. Sasi, S. Sarojam, and S. J. Devaki, High performing biobased ionic liquid crystal electrolytes for supercapacitors, ACS Sustainable Chem. Eng. **4**, 3535 (2016).

[23] A. Labeeb, S. Ibrahim, A. Ward, and S. Abd-El-Messieh, Polymer/liquid crystal nanocomposites for energy storage applications, Polymer Eng. Sci. **60**, 2529 (2020).

[24] A. R. Ibrahim, M. F. Khyasudeen, J. Husband, S. M. Alauddin, N. F. K. Aripin, T. S. Velayutham, A. Martinez-Felipe, and O. K. Abou-Zied, p-methoxy azobenzene terpolymer as a promising energy-storage liquid crystal system, J. Phys. Chem. C **125**, 22472 (2021).

[25] J. Raval, E. Gongadze, M. Benčina, I. Junkar, N. Rawat, L. Mesarec, V. Kralj-Iglič, W. Góźdź, and A. Iglič, Mechanical and electrical interaction of biological membranes with nanoparticles and nanostructured surfaces, Membranes **11**, 533 (2021).

[26] J. C. Phillips, R. Braun, W. Wang, J. Gumbart, E. Tajkhorshid, E. Villa, C. Chipot, R. D. Skeel, L. Kalé, and K. Schulten, Scalable molecular dynamics with NAMD, J. Comput. Chem. **26**, 1781 (2005).

[27] W. Humphrey, A. Dalke, and K. Schulten, VMD – visual molecular dynamics, J. Mol. Graphics **14**, 33 (1996).

[28] K. Górny, V. Raczyńska, P. Raczyński, Z. Dendzik, and S. Starzonek, Impact of polarized nanotube surface on ultrathin mesogen film properties: Computer simulation study, Phys. Rev. E **99**, 022701 (2019).

[29] C. Y. Won and N. R. Aluru, Structure and dynamics of water confined in a boron nitride nanotube, J. Phys. Chem. C **112**, 1812 (2008).

[30] T. K. Mukhopadhyay and A. Datta, Deciphering the role of solvents in the liquid phase exfoliation of hexagonal boron nitride: A molecular dynamics simulation study, J. Phys. Chem. C **121**, 811 (2017).

[31] M. Thomas, M. Enciso, and T. A. Hilder, Insertion mechanism and stability of boron nitride nanotubes in lipid bilayers, J. Phys. Chem. B **119**, 4929 (2015).

[32] Z. Li, Y. Zhang, C. Chan, C. Zhi, X. Cheng, and J. Fan, Temperature-dependent lipid extraction from membranes by boron nitride nanosheets, ACS Nano **12**, 2764 (2018).

[33] T. Darden, D. York, and L. Pedersen, Particle mesh Ewald: An $N\log(N)$ method for Ewald sums in large systems, J. Chem. Phys. **98**, 10089 (1993).

[34] A. Brunger, C. L. Brooks, and M. Karplus, Stochastic boundary conditions for molecular dynamics simulations of ST2 water, Chem. Phys. Lett. **105**, 495 (1984).

[35] P. Dhara and R. Mukherjee, Phase transition and dewetting of a 5CB liquid crystal thin film on a topographically patterned substrate, RSC Adv. **9**, 21685 (2019).

[36] See Supplemental Material at http://link.aps.org/supplemental/10.1103/PhysRevE.108.034702 for the model parameters of 2D substrates, density of the mesogene, parameters of the KWW fit, density profiles of mesogene layers, additional visualizations of the system, and distribution of nematic sample directors for selected layers.

[37] J. K. Sheavly, J. I. Gold, M. Mavrikakis, and R. C. Van Lehn, Molecular simulations of analyte partitioning and diffusion in liquid crystal sensors, Mol. Syst. Des. Eng. **5**, 304 (2020).

[38] S. V. Dvinskikh, I. Furó, H. Zimmermann, and A. Maliniak, Anisotropic self-diffusion in thermotropic liquid crystals studied by ^{1}H and ^{2}H pulse-field-gradient spin-echo NMR, Phys. Rev. E **65**, 061701 (2002).

[39] S. Starzonek, S. J. Rzoska, A. Drozd-Rzoska, S. Pawlus, E. Biała, J. C. Martinez-Garcia, and L. Kistersky, Fractional Debye–Stokes-Eeinstein behaviour in an ultraviscous nanocolloid: glycerol and silver nanoparticles, Soft Matter **11**, 5554 (2015).